

A New Parallel Reservoir Simulation Tool for the Production of Fractured Geothermal Reservoirs

Olivier M. Ricois, Jean-Marc Gratien

IFP Energies nouvelles, 1 et 4 avenue de Bois-Préau, 92852 Rueil-Malmaison, France

olivier.ricois@ifpen.fr

Keywords: Geothermal Fractured Reservoir Simulation, High Performance Computing, Discrete Fracture Networks

ABSTRACT

This paper describes the design, the development, the testing and the applications of a new parallel reservoir modelling research software package dedicated to the production of fractured geothermal reservoirs. The physical and mathematical models are described then the concepts and design principles of the C++ implementation are detailed with a focus on the performance issue.

This research geothermal simulator prototype is based on a parallel computing framework providing advanced generic services to handle in at a high level the complexities related to parallelism, unstructured meshes and linear solvers.

An innovative multiple interactive continua (MINC) flux modelling is used to efficiently simulate heat and fluid flows in fractured geothermal reservoirs. We present different formulations that enable to handle in a same simulation the regional, the reservoir and the well scales while recovering the short term transient state results and also the long term permanent state results. This model has been validated against problems set in the geothermal reservoir engineering code comparison project presented in 1980 and comparative results are presented. Examples of fractured reservoirs have also been simulated on the IFPEN heterogeneous computing cluster facility and the physical results and speedups are discussed.

1. INTRODUCTION

Geothermal Energy has long been regarded as a stable, secure, renewable, non-intermittent and a relatively environmentally friendly energy resource. Deep geothermal exploits natural fluids present at depths, and several types of geothermal energy are ranked according to their temperatures. For heating purposes temperatures of 40°C could be considered (shallow geothermal), for electricity the break-even point is always around 100°C. The usable energy reserve, which can be developed using today's deep drilling technology, is estimated worldwide at around 30 times all fossil reserves (coal, gas and oil). All these types of geothermal energy exploit a deep, naturally warm resource since the Earth is a heat plant.

Deep geothermal energy potential is dependent on the geological context. The fluid temperature gradient may not only be related to conductivity of the rocks, but also, for example, to fluid convection cells established in the fracture network. It is then necessary to have a precise knowledge of the subsurface at the future site in operation. The state-of-practice and emerging trends in geothermal reservoir simulation (Sullivan et al, 2000) pointed out the complexity of the physical process resulting in the coupling of heat and mass transfers in the highly heterogeneous environment of a geothermal reservoir. Often phase changes are involved and the flow is complicated by the presence of additional chemical species such as gases or dissolved salts. Fundamental studies have resulted in a steady advance of the range of physical phenomena that it is possible to include in a geothermal reservoir model, and in improvements in the numerical techniques used in the reservoir simulators. These advances have been quite quickly adopted by geothermal modelers. Thus, some models have used reservoir fluid containing various chemicals and others have included extra features such as a numerical representation of double porosity.

This paper describes the design, the development, the testing and the applications of a new parallel reservoir modelling research software package dedicated to the production of fractured geothermal reservoirs. The code inherits from a strong experience in modelling and simulating the production of oil and gas reservoirs as well as an extensive knowledge and understanding of fractured reservoir specificities. To recover short term transient phenomena and long term permanent state results it is important to simulate precisely well scales, reservoir scales and regional scales. For permanent results we have implemented various models to handle these different scales within a same simulation. In section 2, we present the general governing equations of our model. In section 3, we present numerical features of the software, and the implemented physical models. In section 4, we present our software design that ensure the performance, the modularity and the flexibility required to perform realistic simulations combining the different implemented models and finally in section 5, we validate our approach with test cases issued from the 1980 Geothermal model comparison study and with a realistic study case inspired from the Soultz-sous-Forêt geothermal field in France.

2. GOVERNING EQUATIONS

The modeling of the phenomena involved in the geothermal problem consists in calculating the evolution in space and time of the physical state parameters that describe the fluids of the reservoir domain. These parameters are for instance pressure, temperature, enthalpy, density, composition, saturation,... To do this, the general mass and energy conservation laws as well as some thermodynamic closure equations are used. This system becomes well-posed when the initial and boundary conditions are set appropriately.

2.1 Conservation Equations

The general mass and energy conservation equations are solved on the reservoir domain. The domain is subdivided into finite adjacent connected volumes or grid cells. We hereafter only consider the mass conservation of the water component present either

in water and gas phases depending on pressure and temperature conditions. In case of simulation of tracer components in water or more complex compositional fluids, a similar equation may be written for each component present in the fluids.

For a particular grid cell i , the conservation equation is:

$$V_i \frac{\partial}{\partial t} (\phi_i \sum_{p=w,g} \rho_{i,p} S_{i,p}) - \oint_{\sum_{p=w,g}} (\rho_{i,p} \vec{v}_{i,p} \cdot \vec{n}_{s_i}) dS - Q_i^M = 0 \quad (1)$$

Where V_i is the integrated volume of the cell i bounded by the closed surface S_i , ϕ_i is the porosity, $\rho_{i,p}$ is the molar density of phase p (either water or gas), $S_{i,p}$ is the saturation of phase p , $\vec{v}_{i,p}$ is the apparent velocity of phase p . \vec{n}_{s_i} is a unit vector normal to the surface S_i and pointing outward and Q_i^M denotes a molar source/sink term.

Conservation of momentum is governed by the Navier-Stokes equations, but is normally simplified for low velocity flow in porous media by the semi-empirical Darcy's equation :

$$\vec{v}_p = - \frac{K_{rp}}{\mu_p} \vec{k} (\vec{\nabla} P_p - \hat{\rho}_p \vec{G}_z) = 0 \quad (2)$$

where \vec{k} is the absolute permeability tensor, K_{rp} the relative permeability to phase p and μ_p the dynamic viscosity of phase p , \vec{G} is the vector of gravitational acceleration. $\vec{\nabla} P_p$ and $\hat{\rho}_p$ denote the pressure gradient and the mass density of phase p , and z is the coordinate in the direction of gravity.

The thermal-transport equation is based upon the conservation in a volume element V_i of enthalpies accumulated in fluids and saturated rock:

$$V_i \frac{\partial}{\partial t} [(1 - \phi_i) U_{i,R} + \phi_i \sum_{p=w,g} U_{i,p} S_{i,p}] - \oint_{\sum_{p=w,g}} (H_{i,p} \vec{v}_{i,p} \cdot \vec{n}_{s_i}) dS - \oint \vec{K} \cdot \vec{\nabla} T \cdot \vec{n}_{s_i} dS - Q_i^E = 0 \quad (3)$$

where $U_{i,R}$ denotes the rock volumetric heat capacity (internal energy), $U_{i,p}$ and $H_{i,p}$ are the molar internal energy and molar enthalpy of phase p , \vec{K} is the bulk thermal conductivity tensor and $\vec{\nabla} T$ is the temperature gradient. Q_i^E represents the energy exchange due to sources (negative value) and sinks (positive value) due to the presence of wells, specific boundary conditions or heat losses when the cell volume adjoins with the over-underburden stratum.

Under specific thermodynamic conditions, water and gas phase can coexist in equilibrium in the system. In this case, the pressure and temperature are dependent on each other. Pressure and temperature values are then related with the saturated-pressure relationship:

$$P_w = P_{\text{sat}}(T). \quad (4)$$

The reference phase is the water phase and therefore P_w is the system reference pressure. The pressure of the gas phase P_g is computed as :

$$P_g = P_w + P_{c_{wg}} \quad (5)$$

where $P_{c_{wg}}$ is the capillary pressure of the water-gas system assumed to be a known function of the water saturation. Finally, the saturation closure equation is used to force all the available pores of the rock to be saturated with fluids.

$$S_w + S_g = 1 \quad (6)$$

The temperature T is supposed to be identical in the rock and in the fluids.

2.2 Matrix-Fracture exchanges

Most geothermal reservoirs are naturally fractured with possibly a dense fault network inherited either from a complex tectonic history or a high heat capacity. Two classes of models, the dual medium and discrete fracture models, are commonly used in reservoir simulations to simulate flow and heat transports in fractured porous media. Dual medium models assume that the fracture network is well connected and can be homogenized as a continuum coupled to the matrix continuum using transfer flux functions. On the other hand, discrete fracture models (DFM), represent explicitly the geometry of fractures and faults immersed in the surrounding meshed matrix domain. Due to the complexity to build a numerically acceptable mesh for these types of reservoir geometries, the number of fractures and faults taken into account is limited to a few tens to hundreds. In practical, the model with explicit fracture geometries is expected to reproduce more realistic thermal response curves. However, running these simulation models requires a huge computational cost. There is also high uncertainty in determining the required parameters. As this feature is a key issue for fractured geothermal reservoir modelling, both approaches are available in our prototype simulator.

2.2.1 Dual medium model

This model is based on the Quandalle's approach (Quandalle et al, 1989) where flow exchanges are formulated between matrix blocks and homogenized surrounding fractures. This model is well adapted to handle regional and reservoir scales as it requires few degrees of freedoms per grid cell and it is known to enable to capture well the long term permanent state results. In this approach, a classical Warren & Root dual porosity representation (Warren and Root, 1963) of the matrix and fractures is used, and petrophysical properties of fractures are upscaled at grid cell size (Figure 1).

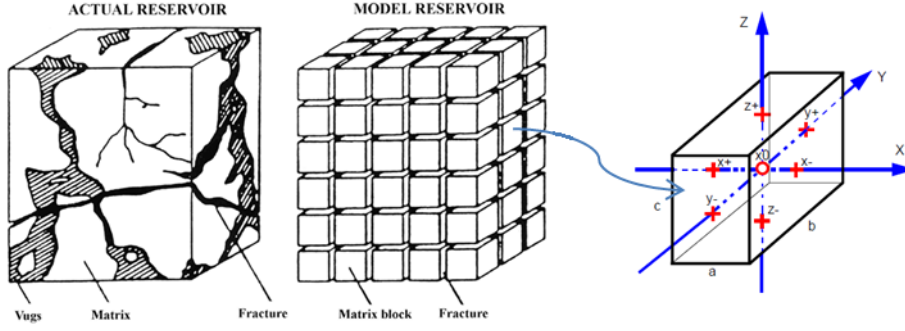


Figure 1: Warren and Root model and Fracture-Matrix flow computations.

The governing equations are written by applying the Darcy law across the six faces of the average schematic matrix block. The block center is "xo", assumed at the grid cell center and where the primary variables are computed both in the fracture and matrix media. The centers of the faces along the X, Y and Z axes are x-, x+, y-, y+, z- and z+ respectively. The flux of a phase through the face i (i = x-, x+ ...) is obtained by writing the Darcy law between the points "xo" and "i". Consequently, the total volumetric flux from the fractures to the matrix block, for each phase is :

$$F^{fm} = \sum_i \left[S_i \times T_i \times \left(\frac{\Phi_i^f - \Phi_{xo}^m}{L_i/2} \right) \right] \quad (7)$$

where T_i the phase transmissivity through the face area S_i , Φ is the phase potential and L_i is the block length in the direction perpendicular to the face i. Superscript f is used for the fracture and m for the matrix block.

The fluxes between the fracture cell and its associated matrix cell are obtained by multiplying the above values (computed for one block) by the number of blocks $N = (d_x \times d_y \times d_z)/(a \times b \times c)$ where d_x, d_y, d_z are the grid cell dimensions.

Assuming the potential continuity at the face i: $\Phi_i^f = \Phi_i^m$, the difference of potential between "i" and "xo" in the matrix may be written, for each phase as :

$$\Phi_i^f - \Phi_{xo}^m = (P_i^f - P_{xo}^m) + (Pc_i^f - Pc_{xo}^m) + \rho_i^m \times g \times (Z_i - Z_{xo}) \quad (8)$$

Where ρ_i^m is the density of the phase computed in the matrix block. The same equation may be written for the difference of potential between "i" and "xo" in the fracture medium:

$$\Phi_i^f - \Phi_{xo}^f = (P_i^f - P_{xo}^f) + (Pc_i^f - Pc_{xo}^f) + \overline{\rho}_i^f \times g \times (Z_i - Z_{xo}) \quad (9)$$

Where $\overline{\rho}_i^f$ is the average phase density in the fracture medium. This last equation is subtracted from the previous one to form :

$$\Phi_i^f - \Phi_{xo}^m = (P_{xo}^f - P_{xo}^m) + (Pc_{xo}^f - Pc_{xo}^m) + (\rho_i^m - \overline{\rho}_i^f) \times g \times (Z_i - Z_{xo}) + (\Phi_i^f - \Phi_{xo}^f) \quad (10)$$

In this formulation, the difference of potential is expressed as the sum of four terms, each representing a physical phenomenon driving the fracture-matrix exchanges.

- $(P_{xo}^f - P_{xo}^m)$ is the expansion term due to the pressure difference in the matrix and fracture media. When, due to production, the pressure decreases in the fractures, the matrix blocks produce by fluid and rock expansion.
- $(Pc_{xo}^f - Pc_{xo}^m)$ is the imbibition term due to the difference in water and gas phase saturations in both media. Capillarity in the fractures is small and very often negligible. Consequently, even low capillary pressures in the matrix may generate appreciable flows, mainly for small size blocks.
- $(\rho_i^m - \overline{\rho}_i^f) \times g \times (Z_i - Z_{xo})$ is the gravity term which only occurs on the z+ and z- faces. This drive mechanism is induced by the difference in fluid density in matrix blocks and surrounding fractures. The gravity force is mainly predominant when the block is vapor surrounded.
- $(\Phi_i^f - \Phi_{xo}^f)$ is the viscous term due to the pressure gradient in the fracture corresponding to the viscous flow in the fractures. Φ_i^f is evaluated by interpolation from the fracture potentials of the neighboring fracture cell centers.

2.2.2 Discrete fracture model

To precisely capture short term transient phenomena, it is important to accurately model the reservoir and well scales. Many works have been conducted on discrete fracture model particularly in the context of the stimulation and production of unconventional oil and gas tight reservoirs. Current efforts (Weng et al. 2014; McClure et al. 2015) concern the development of adapted grid schemes for coupled geomechanical/reservoir models but also reservoir models alone. These models discretize explicitly main flow paths created by fractures instead of using idealized representations such as the universal sugar-box double media representation here above described. This growing interest still encounters challenges when performing simulations for operational-industrial integrated

studies (limited by CPU and memory) and consequently these models are limited to explicit stimulated main fractures to the detriment of information on the natural fracture network.

The lack of satisfying methods for compromising realism and efficiency has inspired an innovative approach: the Discrete and Deformable Fractured Network DDFN methodology, which consists of a special gridding of the fracture network, an aperture management and a simplified geomechanical model. Within the DDFN, fractures are two parallel tortuous planes of small storativity, defined by an aperture, negligible in comparison to fracture characteristic length. An independent pseudo fracture conductivity accounts for laminar fluid flow, following Darcy formalism. Each fracture doesn't need to be finely discretized as transient flow in the fracture medium will be very rapid (few seconds) at the observation scale. So, in the continuous fracture, we placed unknowns only at each fracture intersection. The idea is to consider each intersection as a source term which is reasonable if intersections reflect enhanced zones. Transmissivities along fractures (only one plane relying 2 intersections) are estimated, using an approximate Voronoi diagram in each fracture plane. The fracture medium is by construction continuous from the stimulated wellbore to non-permeable boundaries. The final fracture network mesh benefiting from Voronoi properties is K-orthogonal leading to a conforming mesh, which facilitates simulations. Averaging techniques using electrical rules limit the number of transmissivities and consequently the size of the numerical matrix to solve when border lines become complicated. This approach (named Sweep Line Mesh 3D) has been validated by comparing pseudo-steady state simulations with analytical solutions (Snow, 1969) and finely discretized simulations on a few fractures. The main advantage of the approach is the node number reduction of several orders of magnitude.

The heterogeneous porous matrix continuum is less permeable than primary continuous fracture system. Pressure and temperature gradients in the matrix space, in the vicinity of each fracture, require assessing correctly the exchange surfaces, thus using an adapted scale. Consequently, the choice is to use an octree delineation whose refinement is conditioned by the fracture density. The final octree is equilibrated at the second order.

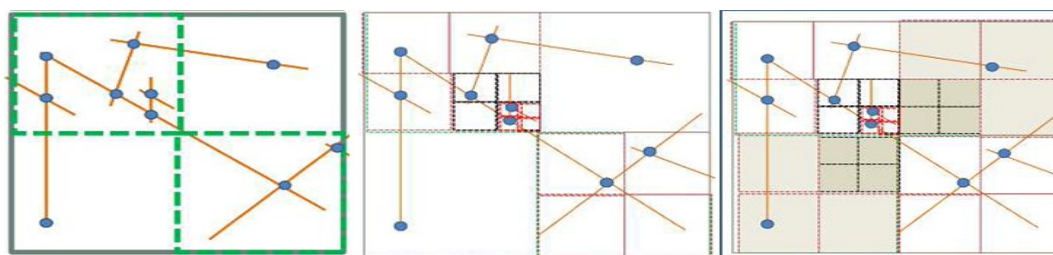


Figure 2: Schematic description of the matrix and fracture meshes. It shows how the octree is spatially adapted to fracture node density (from Khvoenkova & Delorme, 2011).

The reader is invited to consult Khvoenkova & Delorme (2011-2012) and Delorme et al. (2016) for further details on this innovative technology.

2.2.3 Multiple interacting continuum concepts

For geothermal reservoirs producing at a constant flowrate, temperature exchanges start at the matrix/fracture interface and move further into the matrix, as time progresses, very slowly. This transient state can last for several hundred days for reservoirs of very low matrix permeability. To improve transient flow simulation, Pruess, (1983, 1992) and Wu et al. (1988) investigated the multiple interacting continuum concepts (MINC). The MINC method treats inter-porosity flow in a fully transient way by computing gradients which drive inter-porosity flow at the matrix-fracture interface. Matrix blocks are discretized into a sequence of nested volume elements, defined on the basis of distance from the fracture faces, named proximity functions. Analytical expressions of proximity functions can be written assuming regularly 2D or 3D shaped matrix blocks which is the case for the dual continuum models.

In the case of the DDFN models, the proximity functions or namely the transient transfer influence functions are computed in each cell of the matrix medium octree providing a distribution of matrix volume fractions with respect to the nearest natural fracture face distance. As temperature and pressure gradients are very high in the vicinity of fractures, it is very important to finely discretize the matrix surrounding the fracture to capture it accurately. Therefore a logarithmic x-axis is used for the histogram of matrix volume fractions.

A recursive algorithm was developed (Ricois et al, 2016) to compute the transient transfer influence functions. Each matrix octree cell is subdivided by a factor of 2 in each direction (8 sub-cells in 3D). This procedure applies to each of the subdivided cells until no fracture intersects them or if the length of the largest diagonal of the cell is below a threshold value. If the subdivision stops, the volume of the subdivided cell is associated to the distance between its center of mass and the nearest fracture plan (Figure 3).

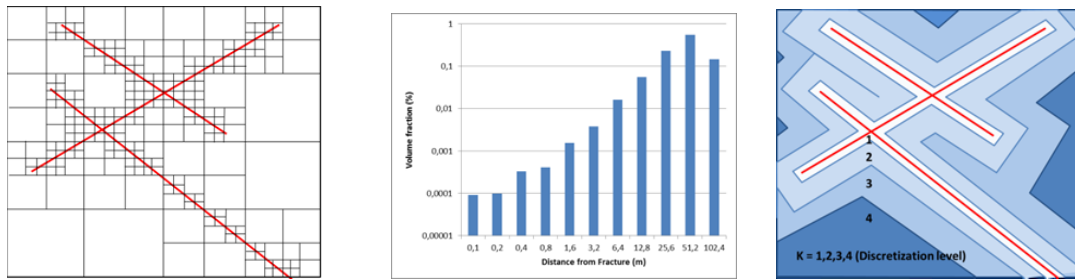


Figure 3: Transient transfer influence function procedure (from Ricois et al., 2016).

Given a chosen width of each nested interacting continua, the transient transfer influence function of each matrix octree cell is used to compute the numerical discretization scheme. The number and the width of nested interacting continua are chosen independently of the transient transfer influence function discretization.

3. DISCRETE FORMULATION

3.1 Variable formulation

The governing equations lead to a system of nonlinear partial differential equations at the continuous level. The system is solved with a first order implicit Euler time discretization and a cell centered finite volume space discretization. The degrees of freedom are chosen as the average values of the thermodynamic state variables (pressure, temperature, saturations, compositions,...) on each grid cells. In our formulation, the size of the system is reduced by choosing a number of primary unknowns and eliminating the secondary ones by the mean of the thermodynamic closure laws. Two options are commonly used in geothermal reservoir simulators. One formulation consists in choosing the pressure, and the temperature as primary unknowns. This scheme is well known to be computationally efficient and easy to implement since thermodynamic properties are derived from pressure and temperature. However it generates numerical difficulties due to non-linearity of enthalpy function at the boundary of the monophasic and the diphasic area. One way to overcome such difficulties consists in introducing the alternative formulation, the pressure-enthalpy-salinity (PHX) scheme (Copol, 2014 and Büsing et al, 2016). This scheme has the advantage to be more stable when the system switches from one phase to two phases.

We adopted a generalized multiphase multicomponent compositional variable formulation based on a Coats type formulation (Coats, 1989) with an innovative enthalpy correlation to stabilize the numerical behavior when the water boiled. Table 1. describes the choice of primary unknowns which depends on a grid cell status indicator updated at the end of each Newton iteration and related to the number of phases present. Under specific thermodynamic conditions, water and gas phase can coexist in equilibrium in the system. In this case, the pressure and temperature are dependent on each other. Pressure and temperature values are then related with the saturated-pressure relationship $P_w = P_{sat}(T)$. Generally, an equation of state for pure water adapted from the International Association for the Properties of Water and Steam (Wagner and Pruss, 2002) is used to compute the saturated pressure as a function of the temperature. In this model, we use values given in tabular form by Schmidt and Grigull (1979) covering the temperature range from 20°C to 370°C.

Table 1: Multiphase multicomponent compositional PTX variable formulation.

status	fluid in presence	primary unknowns	derived unknowns
wg	Water, Gas	P, Sw	T = Tsat(P) Sg = 1-Sw
w	Water	P, T	Sw = 1 Sg = 0
g	Gas	P, T	Sg = 1 Sw = 0
rock	None	T	P, Sw, Sg undefined

The governing fluid flow and heat transport equations are strongly coupled and non-linear, as the coefficients of these equations are non-linear functions of the primary variables. The relative permeability, capillary pressure, gas saturation, density, viscosity and enthalpy of fluids vary strongly with pressure and temperature and are evaluated implicitly. Thus, a robust non-linear algorithm is needed to solve the finite difference approximations. Newton-Raphson's well-known algorithm is used to solve the system of non-linear equations for each time step and to compute the variations of the primary unknowns corresponding to the status of each cell.

3.2 Initial and Boundary Conditions

Understanding heat transport in the subsurface requires assessing the impact of different heat sources on the numerical model. For example, a constant temperature or heat flow is often assigned as the lower thermal boundary condition assuming an average geothermal gradient of 30°C/km beyond the under burden stratum. However, the average geothermal gradient may vary with location. Therefore, assuming a constant geothermal gradient may lead to significant errors if the deep structure is heterogeneous. Furthermore, the natural lateral recharge of the reservoir determines the heat initial distribution but can potentially also impact the production of the geothermal reservoir.

3.2.1 Dirichlet and Neumann boundary conditions

Two boundary conditions have been developed in the model. The Dirichlet conditions specify fluid thermodynamic conditions, such as pressure or temperature on a boundary defined in the model by an arbitrary set of faces of cells. These time-dependent thermodynamic conditions are spatially distributed on the boundary.

A specified heat or fluid flux Neumann boundary conditions can also be directly applied. By default, a zero flux Neumann boundary condition is applied at the boundary of the discretization domain. A fluid flux can also be expressed as a volumetric precipitation (water) flux over the land-surface ($\text{m}^3/\text{m}^2\text{-d}$) to simulate precipitation or recharge boundary conditions.

In both case, for inflow boundary conditions, the nature of the phase (water or steam), the composition, the pressure and temperature of the incoming fluid must be specified to convert the fluid thermodynamic conditions to enthalpy and fluid rates. These enthalpy and molar rates are input implicitly as sink or source terms in the governing conservation equations.

3.2.2 Well model

Intersection of wellbore trajectories with the mesh is computed to defined the perforated cells of the production and injection wells. The well model is derived from a classical steady-state well model in which the well is linked to the reservoir through a geometrical well index (WI) computed with the Peaceman's formula (Peaceman, 2017) and validated for a single phase radial flow on a square grid. The molar water rate for a producer well at perforation i is then expressed as:

$$Q_w^i = WI^i \times \left(\frac{Kr_w^i \times \rho_w^i}{\mu_w^i} \right) \times [P^i - (BHP + \bar{\rho}(z^i) \times g \times (z_{ref} - z^i))] \quad (11)$$

Where WI^i is the geometrical well index input by the user or computed using the the Peaceman's formula, Kr_w^i , ρ_w^i and μ_w^i are respectively the water relative permeability, the molar density and the dynamic viscosity of water computed in the center of cell i at pressure P^i and depth z^i . BHP is the bottom hole pressure of the well measured at well reference depth z_{ref} . $\bar{\rho}(z^i)$ is the explicit average mass density of produced fluids until perforation i . In the case of an injector well, the term representing in the phase mobility in the equation above is computed as the mobility of the injected fluid.

During a time step, the bottom hole pressure of a producer or injector well is either constant (value defined by the user and function of the simulation time) or solved simultaneously with the reservoir unknowns. In the first case, the well is under pressure control. In the other case, the equation above (one per well) is added to the governing conservation equations and the coupling mode resolution is activated for those wells. The BHP is then part of the primary variables solved at each Newton iteration.

The well control mode (pressure or flow rate) is determine at the beginning of each Newton step with an optimization algorithm. This nonlinear optimization problem maximizes the production rates of the wells while honoring the well constraints fixed by the user at that time. There are many different constraints available for a well on operation such as a limit bottom hole pressure, a target water volume rate, a target water mass rate, a maximum pressure drawdown, a target rate for a group of wells, etc. A dichotomous search is used to compute the optimal bottom hole pressure of each well open to flow.

3.3. Water and steam thermodynamic properties

The thermodynamic property laws are introduced according to the variable formulation as closure laws expressed as functions of pressure and temperature.

3.3.1 Molar density

The molar water phase density (in mol/m³) is a function of pressure and temperature, with a salinity dependent corrective term:

$$\rho_w(P, T) = \rho_w(T)[1 + C_w(P - P_{sat}(T))] \cdot f(C_s) \quad (12)$$

Where $P_{sat}(T)$ the saturated-pressure tabular relationship, C_w is a water compressibility, f is a function of water salinity. $\rho_w(T)$ (kg/m³) is correlated with international tables (Schmidt, 1969) at less than 1 % with the relation (P in Pa, T in K):

$$\rho_w(T) = 780.83795 + 1.6269192 T - 3.063354 T^2 \quad (13)$$

The water compressibility (1/Pa) given by (P in Pa, T in K):

$$C_w(T) = a1 + b1 P + T(a2 + b2P) + T^2(a3 - b3P) \quad (14)$$

$$a1 = 2.4638 \times 10^{-9} \quad b1 = -1.1343 \times 10^{-17}$$

$$a2 = -1.2171 \times 10^{-11} \quad b2 = 4.8695 \times 10^{-20}$$

$$c1 = 1.8452 \times 10^{-14} \quad c2 = -5.9978 \times 10^{-23}$$

The salinity depending function is given by:

$$f(C_s) = 1. + 6.5 \times 10^{-4} C_s \quad (15)$$

where C_s is the water salinity given in g/l.

The molar gas phase density (mol/m³) depends on pressure and temperature. The following formulation of the ideal gas equation with compressibility factor correction is used :

$$\rho_g(P, T) = \frac{P}{Z_s RT} \quad (16)$$

Where Z_s is the gas compressibility factor and R is the gas constant. The steam compressibility factor is adjusted from international tables by:

$$Z_s(T) = 1.012 - 4.461 \times 10^{-4} T + 2.9795 \times 10^{-6} T^2 - 1.6631 \times 10^{-8} T^3 \quad (17)$$

3.3.2 Dynamic viscosity

The water dynamic viscosity (in Pa.s) is a function of temperature (in K), water salinity (C_s in g/l) obtained with:

$\mu_w(T, C_s) = \mu_w(T)(1 + 1.34 \times 10^{-3} C_s + 6.12 \times 10^{-6} C_s^2)$ where $\mu_w(T)$ is given by interpolation in international tables. The steam viscosity μ_s is obtained from interpolation in international tables for temperature between 293.15 K and 1003.15 K.

3.3.3 Enthalpy

It is considered (Faust, 1976) that the majority of hydrothermal systems exist below the critical pressure and temperature point. Consequently, empirical equations which determine water enthalpy properties have been developed and are in very good agreement with the data available for pressures below or equal to the saturation pressure when the temperature is below or equal to the critical temperature. However, magmatic hydrothermal systems often operate at near-critical and/or boiling, two-phase conditions. Such conditions pose major computational challenges because of singularities in the equations of state at the vicinity of the critical point. In pressure-enthalpy coordinates, where two-phase conditions are represented as a region rather than a single curve (Figure 4), the relevant properties of liquid water and steam merge smoothly to finite values at the critical point and do not show singularities.

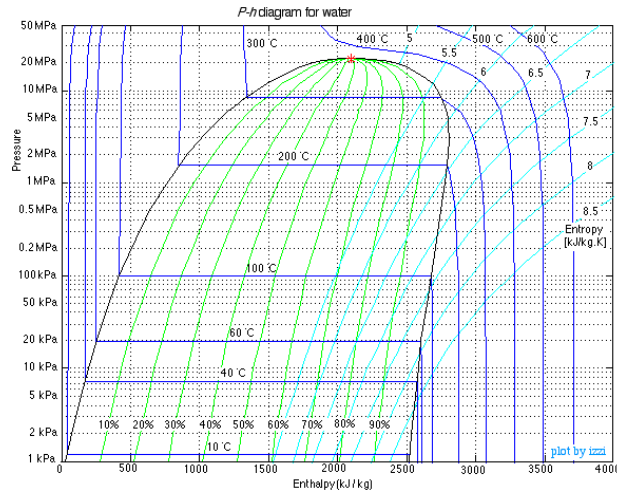


Figure 4: Pressure Enthalpy Diagram for Water and Steam (from NIST Chemistry WebBook - accessed Jan 2008).

A correlation has been developed for the enthalpy of water in liquid or gas phase. When the two phases coexist (saturated state), a correlation giving the latent heat of the water is introduced to ensure the continuity of the water enthalpy model. The ranges of applicability of the model are 0.006108 to 1000 bar for pressures and temperatures from 0 to 800°C.

The enthalpy of liquid or unsaturated vapor water is expressed as a non-linear interpolation (function of pressure and temperature expressed in Bar and °C) between enthalpy at minimum pressure of 0.006108 bar: $H_w^0(T)$ and enthalpy at a pressure of 1000 bar: $H_w^{1000}(T)$. $H_w^0(T)$ and $H_w^{1000}(T)$ are functions of the temperature:

$$H_w(P, T) = H_w^0(T) + f(P, T) \times [H_w^{1000}(T) - H_w^0(T)] \quad (18)$$

For pressures from 0 to 0.006108 bar, the equation is simplified as $H_w(P, T) = H_w^0(T)$. The full equation is only used for pressure from 0.006108 to 1000 bar.

$$H_w^0(T) = hipz + (hupz - hipz) \times \left(\frac{apz \times T_n}{apz \times T_n + 1 - T_n} \right) \quad (19)$$

$$H_w^{1000}(T) - H_w^0(T) = dhipu + (dhupu - dhipu) \times \left(\frac{apu \times T_n^{rupu}}{apu \times T_n^{bpu} + (1 - T_n)^{upu} \times tpu} \right) \quad (20)$$

$$f(P, T) = [1 - ctz \times (P_n - 1)] \times \left[1 - 0.5 \times (1 - P_n) \times \left(1 + \frac{\tan^{-1}\left(\frac{T_n - V_c}{V_c}\right)}{\tan^{-1}\left(\frac{V_c}{V_e}\right)} \right) \right] \quad (21)$$

$$V_c = \frac{T_{sat}}{tu} \quad (22)$$

$$V_e = sia \times P_n \times (1 + sib \times P_n) \quad (23)$$

$$T_n = \frac{T}{tu} \quad (24)$$

$$P_n = \frac{P}{pu} \quad (25)$$

The parameter values used in these equations are:

tu	8×10^2	pu	1×10^3
ctz	3.978557×10^{-2}		
hipz	2.5020×10^3	hupz	4.159×10^3
apz	8.86×10^{-1}	apu	2.08
rpu	1.219	bpu	6.65×10^{-1}
upu	2.81	tpu	3.453
dhipu	2.4063×10^3	dhupu	4.44×10^2
sia	$9.04159132 \times 10^{-2}$	sib	$-1.808318264 \times 10^{-1}$
pcrit	2.212×10^2		

T_{sat} corresponds to the saturation temperature for pressures below the critical pressure. It is also the temperature of the inflection point of the enthalpy curves, when the pressure is above the critical pressure. The correlation used to compute T_{sat} is :

$$T_{sat} = tsc \times (1 - \sqrt{1 - V_b}) - tsd \times \sin \left[\frac{\pi}{tse} \times \text{Log} \left(\frac{P}{tsf} \right) \right] \quad (26)$$

$$V_b = \left(\frac{\exp(V_a^{\frac{1}{3}}) - 1}{tsb} \right)^2 \quad (27)$$

$$V_a = \text{Log} \left(\frac{P}{tsa} \right) \quad (28)$$

where the parameter values used in these equations are:

tsa	6.1080×10^{-3}	tsb	9.0482232
tsc	7.2045764917×10^2	tsd	2.6
tse	5.11	tsf	1.101325

Figure 5 shows that this correlation gives results in conformity with the 1963 international skeleton tables (Burger et al., 1984), as adopted by the Sixth International Conference on the Properties of Steam. It also has the advantage of correctly identifying the point of inflection of the enthalpy curves for pressures above the critical pressure.

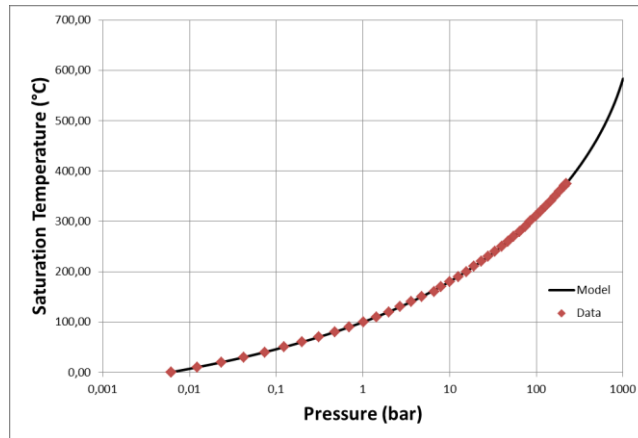


Figure 5: Validation of saturated steam temperature

When the two phases coexist, the enthalpies of each phase can be calculated as follows:

$$H_{vap} = H_w + L/2 \quad (29)$$

$$H_{liq} = H_w - L/2 \quad (30)$$

The latent heat of vaporization L is obtained as a function of temperature by:

$$L(T) = lz \times [(1 - Tpc)^{1/3} - lata \times Tpc \times Vla \times (1 - Vlb^{1/6})^{1/7} \times Vlc] \quad (31)$$

$$Vla = \cos[2\pi \times \text{Log}(1 + 2 \times Tpc)] \quad (32)$$

$$Vlb = (2 \times Tpc - 1)^2 \quad (33)$$

$$Vlc = \text{Exp}(latb \times Tpc^2) \quad (34)$$

$$Tpc = \left(\frac{T}{T_{crit}} \right) \quad (35)$$

where the parameter values used in these equations are:

lata	4×10^{-3}	latb	3.4
lz	2501.0416	T_{crit}	374.15

It is noted that latent heat is equal to 0 at the critical point $T = T_{crit}$ and the derivative of L with respect to T is infinite. This heat latent function is not defined for temperature above T_{crit} .

This enthalpy model has been implemented in our geothermal prototype simulator and the enthalpies of saturated water and steam accurately match the reference data.

4. SOFTWARE ARCHITECTURE

4.1 Arcane and ArcGeoSim framework

Next generation reservoir simulation codes obviously need specific numerical tools in order to be computationally efficient and new advanced physical packages to handle specificities of geothermal reservoirs. Therefore our prototype is based on *ArcGeoSimTM*, a framework dedicated to the development of geoscientific applications (Have, 2015). This framework is itself based on Arcane, a C++-based coding platform (GrosPELLIER & Lelandais, 2009) and enables to design complex multi-physic software seamlessly for parallel hybrid architectures. These combined framework provide through a high level plugin mechanism, a large number of low-level services and advanced numerical tools which can be applied in a transparent way to new business packages designed for geothermal reservoirs. Thus our model could take advantage of new promising approaches including the Adaptive Mesh Refinement (AMR) method (Mesri et al. 2013) with a dynamically refined grid over time to better control the cost and precision of the simulation and a parallel programming model based on a message-passing or task strategy. Linear solvers also include the use of modern architecture such as GPU's on high performance computers (Anciaux et al. 2013-2014-2015). Another obvious benefit of this high performance computing platform is its re-usability of services and increased flexibility with respect to development changes. Examples of geoscientific applications supported by this new platform have been previously reported by Tunc et al. (2012) and Estublier et al. (2014).

To manage the complexity of the different concerns, the structural and geological data representation, numerical methods and physical models, our application has been designed on top of three main orthogonal layers : the Mesh layer, the Numerical layer and the Physical layer. Each of these layers provides a collection of independent modules, services and plug-ins that implement the algorithms. Interfaces ensure the interoperability of these elements.

Specific services or plug-ins were developed to meet the physics of geothermal flows. Each plug-in implements an interface and contains its own data and algorithms that can interoperate with shared mesh structures.

4.2 The Mesh layer

The simulator is designed around a parallel distributed fully unstructured mesh data model. A general mesh module provides geometric entities such as the *Nodes*, *Faces* and *Cells*. These entities are organized in an unstructured representation. The mesh module provides iterators for various collections of entities representing physical regions of the grid. It provides also functionalities to handle the connectivity of the mesh (*Graph*). A *Particle* entity has been introduced to handle clouds of points. Thus a meshless representation of physical fields at a fine scale is possible independently of the scale of the reservoir grid geometry. Adaptive Mesh Refinement or Coarsening methods (Mesri and Ricois, 2015) rely on upscaling algorithms to dynamically compute equivalent property values at each refined or coarse cell based on a fine geological data representation distributed on particles. The *Particle* entity is also used to map the fracture nodes and their associated petrophysical properties.

A simple XML structure holds all what is needed to what makes up the matrix mesh: nodes, facets, cells and relationships between all these geometric elements. Coordinates and properties are stored in separate HDF5 structures referenced in the XML geometry file.

4.3 Degrees of freedom and the Numerical layer

To ensure the orthogonality between Physical, Numerical and Mesh concepts, a Degree Of Freedom (DOF) concept has been introduced. It enables to write numerical algorithms at an algebraic level, manipulating vectors of scalar or tensor quantities, independently of the representation of meshes and geological data. DOFs are abstract entities that can be linked to any mesh or particle entities. These DOFs and their links with mesh entities are computed by numerical scheme services that implement various discretization methods (Two Points Flux, Multi Points Flux Approximation, Finite Element Methods, Virtual Element Methods) provided by the *ArcGeoSimTM* framework, or other specific dual medium transfer functions developed in our application.

In this layer, various models such as multi-phase flow, thermal, and geomechanical models are implemented in separated modules. Different kinds of coupling methods can be considered. The simplest method consists in a one way workflow in which each module updates variables used by the next executed modules. This can be done iteratively with some residual criteria. Some stronger coupling methods can also be considered with fully integrated modules that build a global system with all the physical unknown variables.

4.4 Law concept and the Physical layer

A generic concept of Law enables to implement various physical functions that compute the values of fields discretized on a collection of DOFs. Graphs of Law are built with expressions and compositions of laws. Law evaluations are performed in a vectorial mode for performance reasons. The analysis of law dependencies in the graph enables to update the physical entities only if inputs have changed. Some automatic derivative mechanisms are also available during the Jacobian assembly phase within Newton nonlinear iterations.

4.5 ALIEN and the linear solver layer

Our framework relies on the ALIEN layer, an abstract linear algebraic API to build large sparse linear systems solved with algorithms provided by external linear solver packages like PETSc, Hypre, Trilinos or our in-house IPEN solver package. The ALIEN framework, extensible by a plugin mechanism, enables transformation between various solver package structures. It has a time-stamp mechanism to avoid non necessary memory transfer between local and remote memories (for instance GP-GPU local or pinned memory). At the user application level, the API hides the underlying algebraic structures and makes the application code independent of the evolution of linear solver backends.

5. VALIDATION AND NUMERICAL TEST CASES

We have simulated the problems 4, 5 and 6 of the 1980 Geothermal Model Comparison study (Stanford Geothermal Program, 1980) in order to validate the physical models and the numerical implementation of our prototype. The model settings used are fully described in the original publication. We have finally benchmarked the different discretization models proposed in this paper using a more realistic geothermal fractured reservoir inspired from the Soultz-sous-Forêts geothermal area in France.

5.1 Expanding Two-Phase problem

The purpose of this study case was to simulate a vertical flow of a boiling fluid driven by a combination of gravity and production related pressure gradients. This is a 1D vertical column of water at initial hydrostatic equilibrium conditions. Counterflows of water and steam develop due to the production of water at the bottom and consequently the development of a boiling zone of water in some part of the column. Inflow of cold water is induced at the top. The pressure and liquid saturation profiles are in a perfect agreement with the referenced simulator solutions (Figure 6) demonstrating the capability of our model to handle the counterflow of steam and water, the expansion of a boiling zone and the vertical drainage of cold surface water into a reservoir.

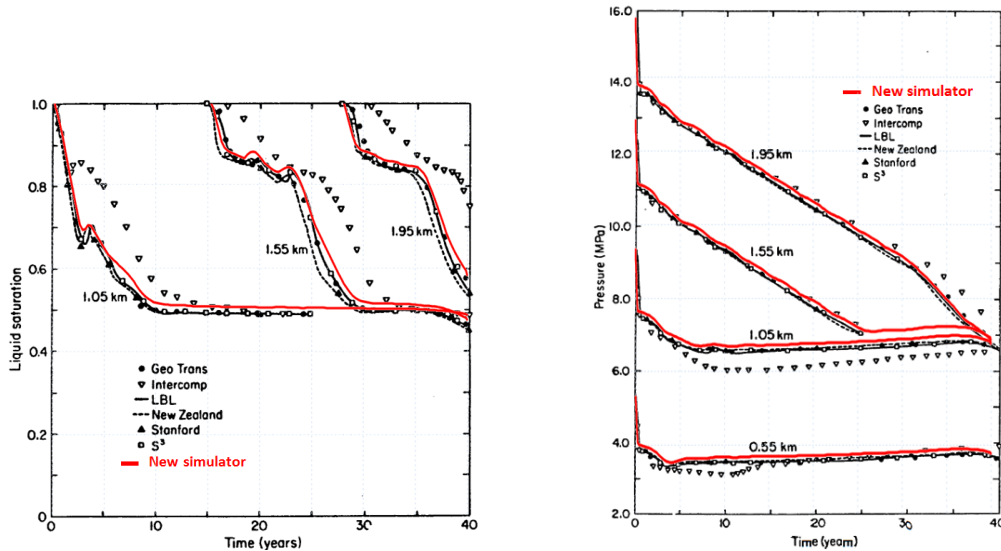


Figure 6: Pressure and water saturation histories at various depths (from Stanford Geothermal Program, 1980).

5.2 2-D Areal Case problem

This test was designed to illustrate the effects of the fluid saturation curve on a simulation model involving both single-phase (water) and two-phase (water/steam) flow with a lateral cold water recharge. A map of initial temperature distribution is given. Two sceneries are simulated, problem A with production only and problem B with production and reinjection of cold water.

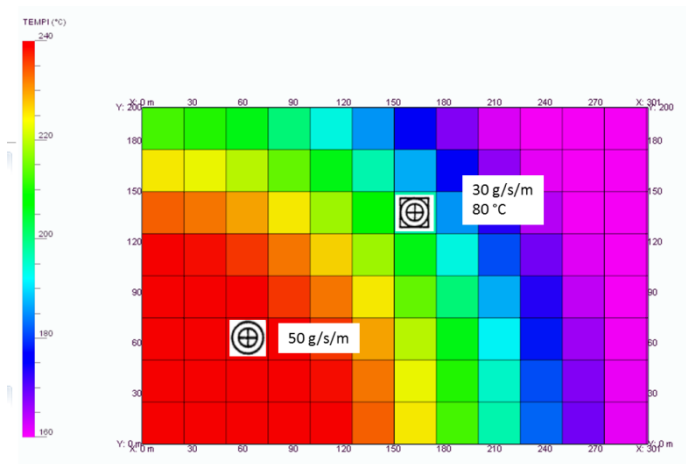


Figure 7: Initial distribution of temperature and location of wells.

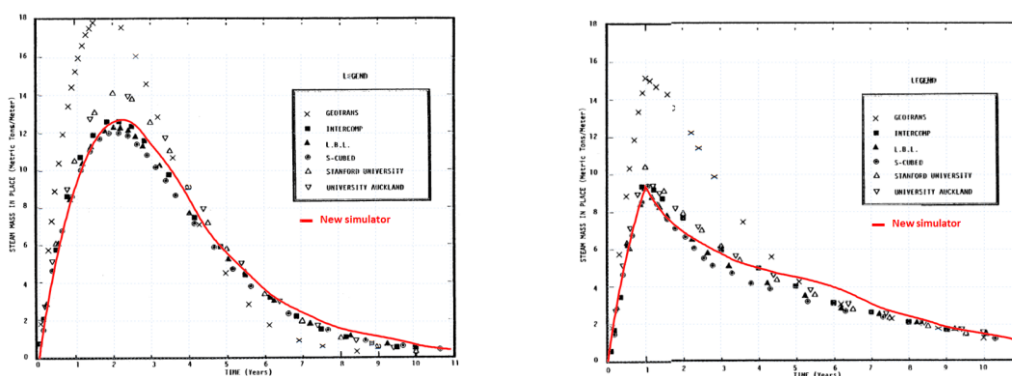


Figure 8: History of total steam in place for problem A (right) and B (left) (from Stanford Geothermal Program, 1980).

The histories of total mass of steam in place for problems A and B shown in Figure 8 is highly correlated to the water-steam saturation curve. Our simulator behaves in the same way as for the referenced benchmark solutions validating an accurate fit of the water/steam saturation curve.

5.3 3D flow problem

This is the most challenging problem of the 1980 Geothermal Model Comparison study. Its design reproduces the three-dimensional nature of geothermal reservoirs and the occurrence of phase transitions with subsequent two-phase flow, including gravitationally induced steam/water counterflow. This 3D synthetic case is inspired from the Wairakei geothermal area in the center of the North Island of New Zealand. The gravitationally equilibrated reservoir is overlain by a immobile two-phase zone and is produced from a well with completions positioned under that zone. Numerical complexity resides in phase transitions and two-phase counterflows. This symmetrical problem is discretized as shown in Figure 9 Dirichlet conditions with constant pressure and temperature are applied at the boundaries of the domain.

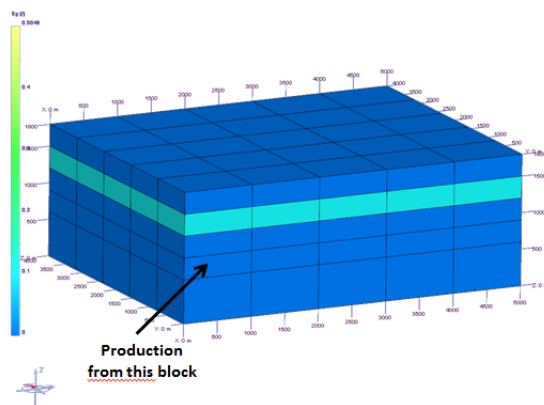


Figure 9: Discretization of the 3D flow problem.

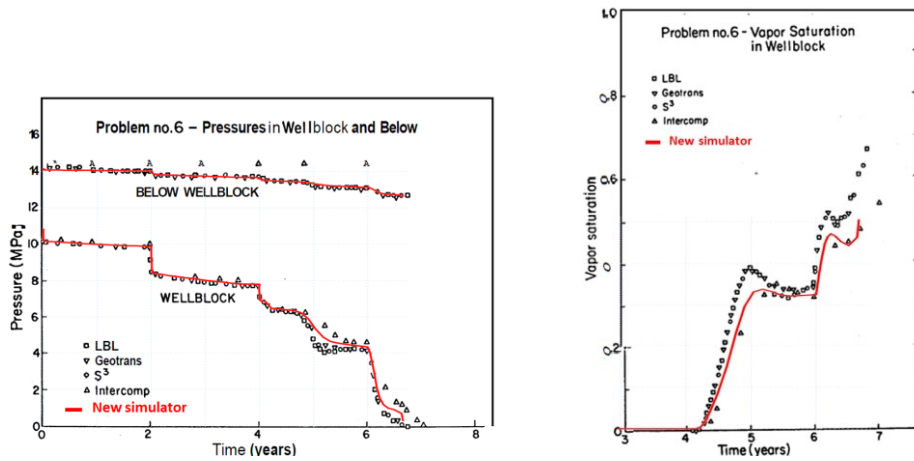


Figure 10: Discretization of the 3D flow problem (from Stanford Geothermal Program, 1980).

The Figure 10 compares the performance of our code with the referenced solutions. Here again it shows a good quantitative agreement between the different codes and demonstrates the ability to compute a difficult 3D depletion problem, involving phase transitions, gravitationally induced steam water counterflows, and recharges.

5.4 Synthetic fractured geothermal reservoir

We built a geothermal fractured reservoir inspired from the Soultz-sous-Forêts geothermal area in France (Genter et al, 1997) in order to test the different discretization approaches available for fractured geothermal reservoirs. The purpose of this preliminary work was not to match the production of this model but to study and try to understand the differences between the approaches in order to establish the best practices and recommendations for the users. We hereafter only describe the discretization of the models and the results of the simulations because this study is still an ongoing research project.

Figure 11 shows the conceptual general organization of the fault system of the reservoir. Major faults have antithetic orientations relative to the domain border and natural fracture zones develop antithetic to major faults. The two wells intersect the major fault plans.

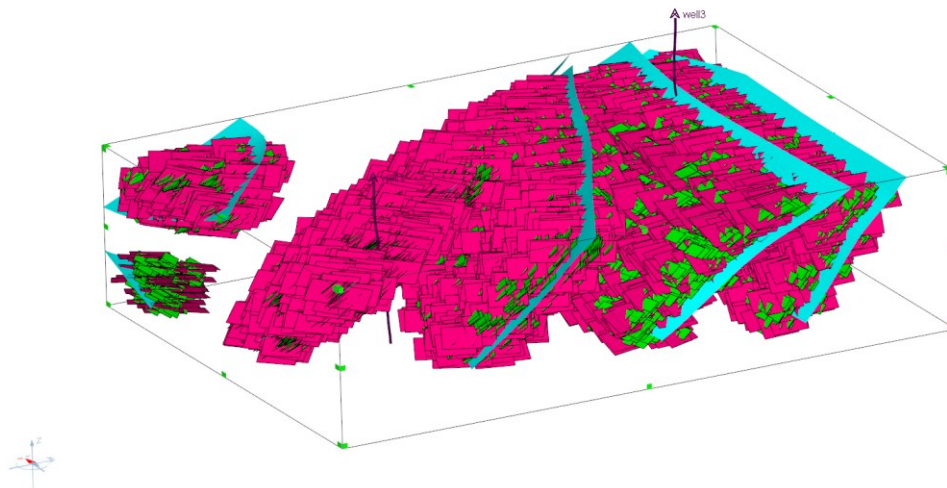


Figure 11: Fracture characterization and Discrete Fracture Model.

Figure 12 shows the discretized models built to simulate the production of this geothermal reservoir. The two approaches available in our simulator were used. The dual medium corner point grid (21x15x10) has 3150 active matrix cells but actually only 921 active fracture cells as the fractured zone extends only around the major faults. The petrophysical properties of fracture cells are upscaled from the fracture conceptual model characteristics. The DDFN discretization has half a million degrees of freedom (387792 active fracture nodes and 14805 matrix nodes). Fracture nodes (represented as a cloud of points in Figure 12) are located at the intersection of natural fracture planes of the discrete fracture model. Transmissivities between the fracture nodes are computed according to aperture and conductivity of the natural fractures.

For both discretizations, the MINC concept is applied to discretize the matrix blocks in order to better capture the temperature front in the matrix. For the dual medium model, the MINC scheme pattern is defined as a percentage of total volume of the matrix cell given for each nested interacting continuum. In this model, 5 nested interacting continua were generated for each matrix cell with the following sequence (0.01;0.05;0.1;24;6), that is the innermost nested subgrid contains 60% of the total matrix volume.

For the DDFN model, the number and the width of nested interacting continua define the MINC pattern. In this example, the nested subvolumes are distributed in the following sequence (0.01;0.5;1;3;5;10;20;50;100) away (in meter) from the nearest fracture plane.

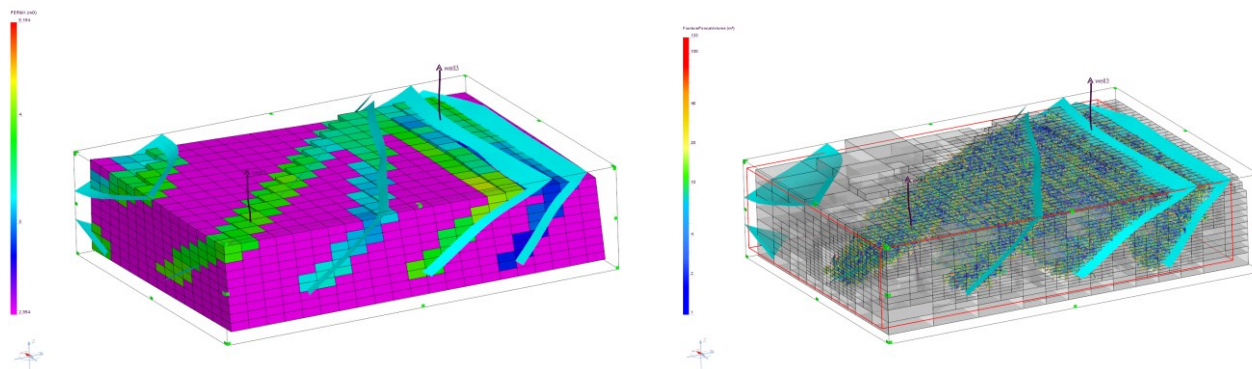


Figure 12: Discretizations of the geothermal reservoir : Dual medium (left) and DDFN (right) models.

The initial temperature of the reservoir is set to 160°C. Hot water is produced during ten years at Well3, and cold water (60°C) is injected at Well1. The two wells operate at a constant rate of 3000 t/d and the injected fluid at Well1 is traced in the reservoir. In Figure 13, We compare the concentration of the injected fluid measured at the production well during the simulation for the two discretization approaches.

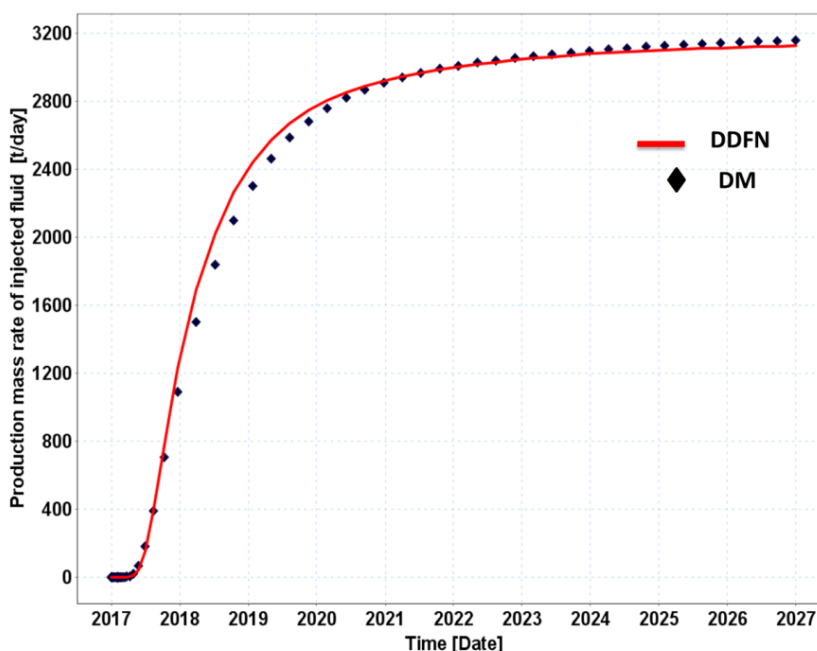


Figure 13: Production mass rate of injected water (t/d).

An injected water breakthrough is observed after one year of simulation. It is the proof of a favorable flow path between the two wells due to the presence of natural fractures at the vicinity of the major faults. However, the temperature at the production well remains at its original value.

The DDFN approach is supposed to give the reference solution. However in this case, the two discretizations perform the same way as the permanent state is correctly simulated with an upscaled dual medium approach. This is mainly because the high ratio between the matrix block size (about 20 m) and the cell dimensions (300m) is favorable to the homogenization algorithm of the fracture petrophysical properties used in the dual medium discretization. Higher matrix block sizes (synonym for lower a fracture density) will introduce significant errors for the dual medium approach.

In Figure 14, we bring out the effects of the MINC concept on the simulation results for both discretizations.

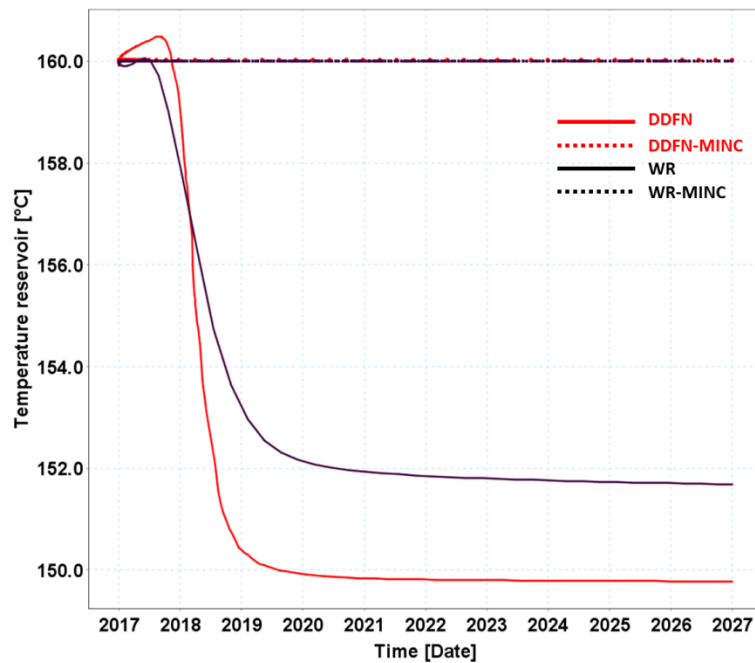


Figure 14: Reservoir temperature at production well.

The red curves show the evolution of the average temperature in the reservoir in the vicinity of the production well for the DDFN model with and without application of the MINC matrix discretization concept and the black curves are for the dual medium model. The heating of the fracture fluid is underestimated without application of the MINC scheme because the temperature gradient in the matrix is not accurately captured. This has a significant impact on the temperature front and consequently on the performance of a geothermal reservoir. Using the MINC scheme, the heat exchange between the matrix and the fractures are correct and both discretizations give the same constant temperature at the production well.

In Figure 15, the first year of the simulation is zoomed to highlight the transient state period. The water coming from the fracture and the matrix media is traced separately and production mass well rate is plot for each water. The DDFN and dual medium discretizations give significantly different results. The dual medium discretization overestimates the production of water coming from the matrix media and the kinetic of production of this water is completely different. This could be explain by the difference in the surface of exchange between the matrix and the fracture media in the two discretization models.

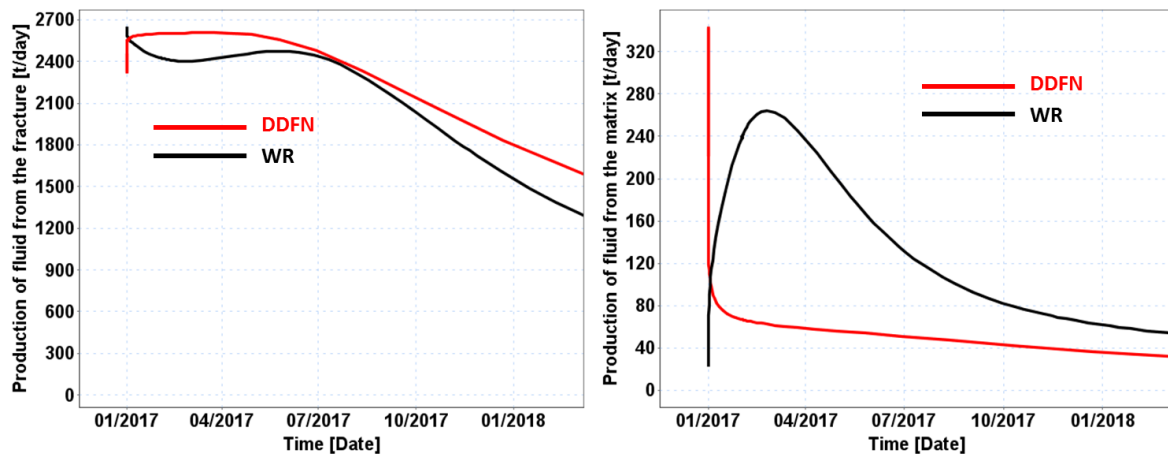


Figure 15: Reservoir temperature at production well.

Because of the difference in the number of degrees of freedom, the DDFN discretization models require higher CPU times to run. To be competitive, it should be run on a cluster hardware to get benefit from a multicore architecture.

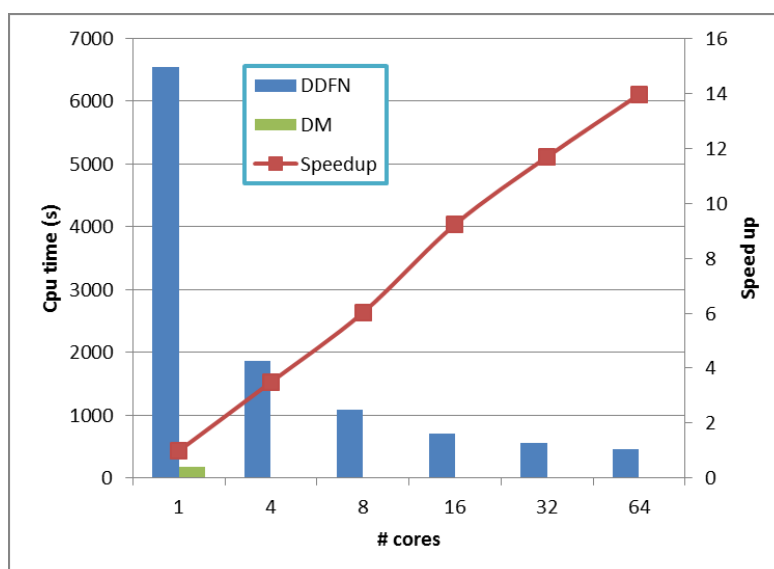


Figure 16: Comparison of CPU times and speed-ups.

Figure 16 gives CPU times of the different simulations run on ENER220, the new IFPEN parallel supercomputer (225 Tflops for 120 nodes with 2x18 compute cores on each node). The dual medium discretization is very competitive but the DDFN approach when run in parallel can actually be used with reasonable cpu times to simulate a geothermal reservoir. The optimal number of cores depends on the number of degrees of freedom of the model. In this example, with half a million nodes, 32 compute nodes is a good compromise.

6. PERSPECTIVES AND ONGOING RESEARCHES

In this work, we validate the formulation and results of our simulation prototype. The dual medium formulation inherited from a long past experience in oil and gas reservoir simulation and associated with a MINC meshless numerical discretization of the matrix cells can simulate the production of hot water and the thermal front advancement in a geothermal fractured reservoir. The DDFN innovative new discretization, based on the actual complexity of the geology and natural fracturing characterization, offers a potentially predictive model which still need to be investigated on actual fractured geothermal reservoir. A simplified hydro-thermal-mechanical-chemical model using the DDFN discretization is currently under development to account for the thermal stress variations caused by injection/production operations.

7. CONCLUSIONS

We introduced a new parallel reservoir simulation tool for the production of fractured geothermal reservoirs based on a Coats type formulation, coupled with the conductive and convective transfers of energy. A dual medium formulation, highlighted the physical phenomena driving the fracture-matrix exchanges is discussed. A new discretization for fractured geothermal reservoirs, based on actual natural fracture geometries is able to effectively handle industrial-scale predictive models at reasonable computation costs. The code takes advantage of an advanced and high performance C++ based simulation framework, that insure interoperability and provide also for non-programmer scientists a fast and reliable way of prototyping physical models dedicated to the geothermal issues. We have validated the results of our simulator against standard academic models from the geothermal domain. Finally, using a realistic study case reservoir inspired from the Soultz-sous-Forêts geothermal area in France, we have demonstrated the interest of our approach based on original numerical formulations and dedicated to handle efficiently at the same time transient state phenomena at the well and reservoir scales and long term phenomena at the regional scale within a reasonable computation time.

REFERENCES

- O'Sullivan, Michael & Pruess, Karsten & J. Lippmann, Marcelo (2000). State of the art geothermal reservoir simulation. *Geothermics*. 30. 395-429. 10.1016/S0375-6505(01)00005-0.
- Quandalle, P., & Sabathier, J. C. (1989). Typical Features of a Multipurpose Reservoir Simulator. Society of Petroleum Engineers. doi:10.2118/16007-PA
- Warren, J.E. and Root, P.J. (1963). - The Behavior of Naturally Fractured Reservoirs.- SPE J. 3 (3): 245–255. SPE-426-PA.
- Weng, X., Kresse, O., Chuprakov, D., Cohen, C. E., Prioul, R., & Ganguly, U. (2014). Applying complex fracture model and integrated workflow in unconventional reservoirs. *Journal of Petroleum Science and Engineering*, 124, 468-483.
- McClure, M., Babazadeh, M., Shiozawa, S., & Huang, J. (2015, February 3). Fully Coupled Hydromechanical Simulation of Hydraulic Fracturing in Three-Dimensional Discrete Fracture Networks. Society of Petroleum Engineers. doi:10.2118/173354-MS.
- Snow, D. T. 1969. Anisotropic Permeability of Fractured Media, *Water Resource Research* 5 (6): 1273 – 1289. DOI: 10.1029/WR005i006p01273.
- Khvoenkova, N., & Delorme, M. (2011, September). An optimal method to model transient flows in 3D discrete fracture network. In IAMG conference (pp. 1238-1249). DOI: 10.5242/iamg.2011.0088.

- Khvoenkova, N., and Delorme, M. (2012). Method for generating a fractured reservoir mesh with a limited number of nodes in the matrix medium. U.S. Patent Application 13/644,479.
- Delorme, M., Bossie-Codreanu, D., Ben-Gharbia, I., Khebzegga, O., Khvoenkova, N., Ricois, O. (2016). Unconventional Production Forecast needs Integration of Field Hydraulic Stimulation Data through Fracture Model Calibration and Optimized Numerical Scheme. Society of Petroleum Engineers. SPE180946-MS; DOI: 10.2118/180946-MS
- Pruess, K.. 1983. Heat Transfer in Fractured Geothermal Reservoirs with Boiling, *Water Resources Research*, 19, (1) 201-208, February.
- Pruess, K. (1992). Brief Guide to the MINC—Method for Modeling Flow and Transport in Fractured Media. Earth science division. Lawrence Berkeley Laboratory, University of California, Berkeley.
- Wu, Y.-S., and Pruess K. (1988), A multiple-porosity method for simulation of naturally fractured petroleum reservoirs, *SPE Reservoir Eng.*, 3, 327–336.
- Ricois, O. M., Gratien, J-M., Bossie-Codreanu, D., Khvoenkova, N., & Delorme, M. (2016, November 12). Advantages of an Unstructured Unconventional Fractured Media Model Integrated Within a Multiphysics Computational Platform. International Petroleum Technology Conference. doi:10.2523/IPTC-18846-MS
- Copol, C., Laminie J., Lopez, S.,. Numerical modeling of geothermal systems (2014). 39th Workshop on Geothermal Reservoir Engineering, Feb 2014, Stanford, United States. pp.SGP-TR-202, 2014. <hal-00944133>
- Büsing, Henrik & Niederau, Jan & Clauser, C. (2016). Pressure-enthalpy formulation for numerical simulations of supercritical water/steam systems applied to a reservoir in Tuscany, Italy.
- Coats, K. H. (1989, January 1). Implicit Compositional Simulation of Single-Porosity and Dual-Porosity Reservoirs. Society of Petroleum Engineers. doi:10.2118/18427-MS
- Wagner, W and Pruss, A (2002). The IAPWS Formulation 1995 for the Thermodynamic Properties of Ordinary Water Substance for General and Scientific Use," *J. Phys. Chem. Ref. Data*, 31, 387-535
- Schmidt, E. & Grigull, U., 1912- (1979). Properties of water and steam in SI-units : 0-800 C, 0-1000 bar (2nd, rev. and updated, printing edited by Ulrich Grigull). Springer-Verlag, Berlin
- Schmidt, E. (1969). Properties of Water and Steam in SI-Units. Berlin: Springer-Verlag.
- Faust, C. R. (1976). Numerical simulation of fluid flow and energy transport in liquid and vapour dominated hydrothermal systems, PhD Thesis, Pennsylvania State Univ.
- Burger J., Souriau P., Combarous M. (1984). Récupération Assistée du Pétrole - Les méthodes thermiques. Editions Technip, Table 2.I.c page 2.7.
- Have, P. (2015) Arcane/ArcGeoSim, a software framework for geosciences simulation. <http://orap.irisa.fr/wpcontent/uploads/2015/11/ORAP-2015-Have.pdf>
- Grospellier G., and Lelandais B.. (2009). The Arcane development framework. POOSC'09, 8th workshop on Parallel/High-Performance Object-Oriented Scientific Computing.
- Anciaux A., Gratien J-M, Ricois O. M., Guignon T., Theveny P., and Hacene M. (2014). Enhanced Oil Recovery simulation Performances on New Hybrid Architectures. GPU Technology Conference 2014. GTC 2014 - ID S4373.
- Anciaux-Sedrakian A., Gottschling P., Gratien J-M., and Guignon T. (2013). Survey on efficient linear solvers for porous media flow models on recent hardware architectures. *Oil & Gas Science and Technology – Revue d'IFP Energies nouvelles*. doi:10.2516/ogst/2013184.
- Mesri Y., Gratien J-M., Ricois O., and Gayno R., IFPEN. (2013). Parallel Adaptive Mesh Refinement for Capturing Front Displacements: Application to Thermal EOR Processes. 09/2013; DOI: 10.2118/166058-MS.
- Anciaux-Sedrakian A., IFP Energies nouvelles; Eaton J., NVIDIA; Gratien J-M., Guignon T., Havé P., Preux C., and Ricois O., SPE, IFP Energies nouvelles. (2015). Will GPGPUs be Finally a Credible Solution for Industrial Reservoir Simulators? SPE 173223: DOI: <http://dx.doi.org/10.2118/173223-MS>.
- Tunc X., Faille I., Havé P., Cacas-Stentz M.C. and Gallouet T. (2012). : A model for conductive faults with non-matching grids - *Computational Geosciences*, Vol 16, n° 2, pp 227-296, Springer.
- IPTC-18846-MS 27 Estublier, A. Michel, Bachaud P., Maurand N., and Deflandre J.P. (2014). Long term fate of CO2 in a saline aquifer : modelling issues - *Computers and Mathematics with Applications*, Vol. 68, No 12, Part B, 2014, pp. 3464-3474–2347, 2014, Elsevier.
- Mesri Y., Ricois O. Method of constructing an optimized mesh for reservoir simulation in a subterranean formation. United States, Patent n° : US2015323701 (A1) 2015, 14 p. (hal-01651785).
- Peaceman, D. W., (1977). Interpretation of well-block pressures in numerical reservoir simulation, SPE 6893, 52nd Annual Fall Technical Conference and Exhibition, Denver.
- Stanford Geothermal Program (SGP) (1980). Proceedings of the Special panel on Geothermal Model Study, Report SGP-TR-42, Stanford University, Stanford, CA.

Genter A., Traineau H., Artignan D., (1997). Synthesis of geological and geophysical data at Soultz-sous-Forêts (France). Rapport BRGM R 39440, p.36.